EAST EUROPEAN JOURNAL OF PHYSICS. **2.** 319-331 (2026)
DOI:10.26565/2312-4334-2026-2-33 ISSN 2312-4334

MHD DUCT FLOW OF NANOFLUID INFLUENCED BY A DUAL HEAT SOURCE IN THE PRESENCE OF AN ELECTRIC FIELD (E_o) AND A MAGNETIC FIELD (B_o)

Bishnu Ram Das[1], Hirak Jyoti Dehingia[2], Kaushik Dehingia[3,4], Rupjyoti Borah[5], Utpal Saikia[6]
[1]*Department of Mathematics, BCM College, Kamrup-781102, Assam, India*
[2]*Department of Basic Science and Humanities, DUIET, Dibrugarh University, Dibrugarh, Assam, India, 786004*
[3]*Department of Mathematics, Sonari College, Charaideo, Assam, India, 785690*
[4]*Research Center of Applied Mathematics, Khazar University, Baku, Azerbaijan, AZ1096*
[5]*Department of Mathematics, Tingkhong College, Tingkhong-786612, Dibrugarh, Assam, India*
[6]*Department of Mathematics, Golaghat Polytechnic, 785610, Furkating, Golaghat, Assam, India*
Corresponding Author email: hirakjyotidehingia11@gmail.com
Received February 11, 2026; revised April 26, 2026; accepted May 8, 2026

The flow of copper (Cu), silver (Ag), titanium oxide (TiO_2), copper oxide (CuO) nanoparticles with water as a base fluid in the presence of a high magnetic field in a vertical rectangular duct are examined in this research. The duct's left and right walls are kept at various steady temperatures and concentrations. The temperature, velocity, and nanoparticle concentration fields are all described by the transport equations. The second-order upwind method, an explicit finite-difference method (EFDM), is used to discretize the coupled nonlinear Navier-Stokes equations. To examine the heat transfer efficiency of this nanofluid, we nondimensionalized the governing equations and obtained solutions using an explicit numerical scheme. MATLAB code is used to perform computational steps. We have plotted the velocity, temperature, and concentration fields for different values of the magnetohydrodynamic (MHD) flow parameters, including the thermal Grashof number (G_r), solutal Grashof number (G_c), Hartmann number (H_a), electrical field load parameter (E), Brinkman number (B_r), and nanoparticle volume fraction (ϕ).
Keywords: *Electrical field; Magnetic field; Nanofluids; Nonlinear; Explicit finite difference technique (EFDT); Rectangular vertical duct; MHD flow; Buoyancy force; Viscous flow*
PACS: 44.20.+b, 44.40.+a, 44.30.+v, 47.11.-j, 47.11.Bc

1. INTRODUCTION

Smooth restraint of convective transport phenomena is a significant challenge across diverse fields of engineering, and biomedical devices that absorb magneto-hydrodynamics (MHD) coupled with Multiphysics. MHD convective transport has broad applications in industry and engineering and is advancing rapidly in medical sciences. Thermal aspects are closely connected to bio-heat and thermal treatment in various tumors. Targeted drug delivery, imaging, and the use of nanoparticles during chemotherapy are well-established. MHD convection is widely used in biomedical technology for magnetic endoscopy, cell separation, tumor treatment and cancer therapy, targeted drug delivery in the body, blood flow control during medical surgery, control of gastrointestinal disorders, transport of complex bio-waste fluids, etc. Adding nanoparticles into the base fluid is an innovative way to enhance heat transfer. The resulting mixture of base fluid and nanoparticles, which has unique physical and chemical properties, is referred to as a nanofluid. Nanofluids exhibit better suspension stability, Newtonian behavior, and enhanced thermal conductivity, and the chaotic motion of nanoparticles is responsible for the enhancement of heat transfer. In natural convection studies, the base fluid has low thermal conductivity, limiting heat transfer enhancement. Researchers applied the innovative technique using nanofluids with higher conductivities to enhance heat transfer. Firstly, Choi studied nanoparticles in 1995 and the base fluid [1, 2] at the Argonne National Laboratory in the U.S.A. After that, the idea has been extended [3] to incorporate an additive nanoparticle into a base fluid to increase the thermal conductivity of the interruption. Many authors [4-6] have reported that thermal conductivity can be enhanced by about 20% at very low volume fractions (1-5%). Thermal conductivity of copper-water nanofluid up to 7.5% of nanoparticle volume fraction empirically determined by Xuan *et al.* [6]. Many authors [7-12] have studied the increase in heat transfer with nanofluids. Tavman *et al.* [13] reported in 2010 a considerable increase in the viscosity of a nanofluid containing aluminum oxide, titanium oxide, and silicon oxide nanoparticles in water. As in the Einstein representation [14], they also show that the traditional verifiable hypothesis, that intellectual investigation of specific heats is minimal for nanofluids, is also true. Namburu [15] in 2009 studied that ethylene glycol-based nanofluids demonstrated lower specific heat than their individual base fluids. Likewise, Bergman [16] confirmed that a water-based aluminum oxide nanofluid exhibited increased thermal conductivity, but only when the specific heat was lower than that of the base fluid. Magnetohydrodynamics (MHD) plays a significant role in nanofluid flow, owing to its expanding industrial applications and use in reactor cooling analysis. Younsi [17] has studied double heat-source magnetohydrodynamics (MHD), which is essential for the material-freezing process. Sharma and Singh [18] and Vadher et al. [19] investigated electrically conducting fluid oiling, the concept of coating synthesis, the salvation of liquefied metals, and active, etc.

Several authors have studied magnetohydrodynamic (MHD) flows and heat transfer in rectangular ducts. In an earlier numerical study [20], the characteristics of different metallic nanofluids with cooling provided by a constant-

Cite as: B.R. Das, H.J. Dehingia, K. Dehingia, R. Borah, U. Saikia, East Eur. J. Phys. 2, 319 (2026), https://doi.org/10.26565/2312-4334-2026-2-33

temperature wall were studied. In another study, Ellahi *et al.* [21] considered a water-based nanofluid with Al_2O_3. To study the aggregation effect on such a nanofluid, Hamad [22] investigated the analytical solution for natural convection flow of a nanofluid over a similar drawing out in the presence of a magnetic field. Mixed convection of Casson nanofluid over a stretching sheet with convectively heated heat source/sink and chemical reaction observed by Hayat *et al.* [23]. Kameswaran *et al.* [24] studied hydromagnetic nanofluid flow owing to a stretching or shrinking sheet. Boundary layer flow of a nanofluid past a stretching sheet with a convective boundary condition studied by Makinde and Aziz [25]. Beg *et al.* [26] investigated the calculation of thermo-solutal convection with Soret-Dufour cross-diffusion in a vertical duct filled with metallic/carbon nanofluids. Nadeem *et al.* [27] studied the magnetohydrodynamic (MHD) three-dimensional layer flow of a Casson nanofluid past a linearly stretching sheet with convective boundary conditions. Abu-Nada and Oztop [28] have numerically investigated free convection in a partially heated rectangular duct saturated with nanofluids. Rashidi *et al.* [29] studied the buoyancy effect on magnetohydrodynamic (MHD) flow of a nanofluid over a stretching sheet in the presence of thermal radiation. Simulation of magnetohydrodynamics (MHD) convective heat transfer and copper-oxide/water nanofluid flow considering Lorentz forces discussed by Sheikholeslami *et al.* [30]. Turkyilmanzoglu [31] has examined the natural convection flow past an impulsive, radiative vertical plate. Very recently [32], Rao and Deka studied the transport phenomena in a nanofluid under the action of a transverse magnetic field. In a vertical square rectangular duct, Das *et al.* [33] numerically investigated the magnetohydrodynamics (MHD) miscellaneous displacement flow of $Al_2O_3 - water$ nanofluids. Many authors who have recently studied the heat transfer nanofluid boundary-layer problem are listed in the reference [34-36].

The goal of our present work is to investigate the flow of copper (Cu), Silver (Ag), Titanium oxide (TiO_2), and Copper oxide (CuO) nanoparticles with water (H_2O) in a rectangular vertical duct, the non-dimensional conservation equations are strongly nonlinear and are solved numerically. Appropriate values of the flow parameters are considered for investigation. The numerical results are presented graphically, including velocity, temperature, concentration, and flow parameters. Utilize the MATLAB code estimation procedure to implement.

Table 1. Thermo-physical numerical values of water (H_2O) and nanoparticles copper (Cu), silver (Ag), titanium oxide (TiO_2), and copper oxide (CuO)

Nanoparticle/base fluid	Density (ρ)	Specific heat capacity (C_p)	Thermal conductivity (k)	Electrical conductivity (σ)
H_2O	997.1	4179	0.613	5.5×10^{-6}
Cu	8933	385	401	59.6×10^{6}
Ag	10490	235	429	6.30×10^{7}
TiO_2	4250	686.2	8.9528	2.58×10^{-7}
CuO	6310	530	20	10^{-5}

2. MATHEMATICAL FORMULATION

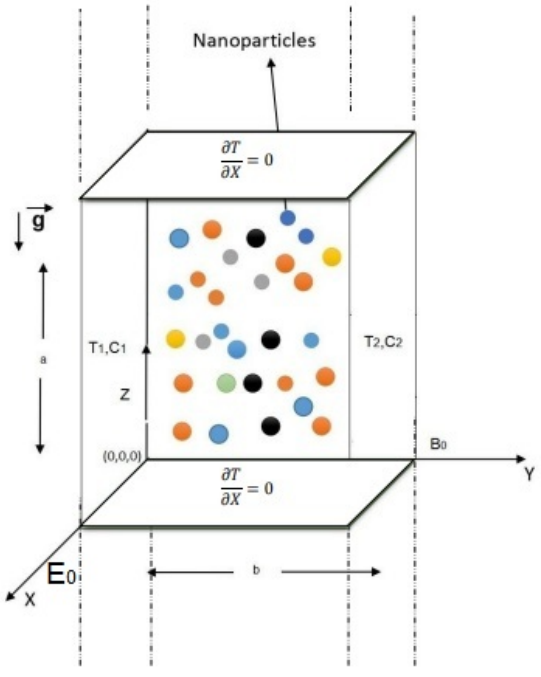

Figure 1. Schematic diagram of the problem

In this model, we have considered a laminar steady flow of incompressible fluid through a duct which is vertically positioned, and the $Z-$axis of the reference frame is along the duct $Y-$axis, taken along the magnetic field B_0, is sufficiently strong and acting normally on the surface of the duct, and the $X-$axis taken along the electrical field E_o. The model of the present problem is shown in Fig. 1. $\overrightarrow{g}$ is the gravitational acceleration, acting downward. The heat source for the flow is taken to be the left duct wall, which is maintained at a constant temperature T_1 with concentration C_1. Similarly, the other heat source is taken as the right duct wall, which is kept at a constant temperature, T_2 on C_2. The right fence is hotter than the left wall, so in this case, $C_2 > C_1$. Here, we have considered prime a to be the length and prime b to be the breadth of the vertical rectangular duct. The well-known Boussinesq approximation is adopted. To get convergent solutions, the Successive-Over-Relaxation (SOR) method, along with the Gauss-Seidel method, was implemented to solve the reduced difference equations.

The following assumptions are made in this study:

- Laminar steady flow of incompressible fluid through a duct.
- The flow field is exhibited through the Velocity profile in the mesh (x, y, v); Temperature profile in mesh (x, y, T) and the concentration profile in the mesh (x, y, c) for copper nanoparticles.

Governing equations

Equation of continuity:

$$\nabla \cdot \vec{V} = 0. \tag{1}$$

MHD momentum equation:

$$\rho_{nf}\left[\left(\vec{V}\cdot\nabla\right)\vec{V}\right] = \mu_{nf}\nabla^2\vec{V} + \vec{g}(\rho\beta)_{nf}(T-T_o) + \vec{g}(\rho\beta)_{nf}(C-C_o) + \left(\vec{J}\times\vec{B}\right) + \sigma_{nf}B_o^2E_o. \tag{2}$$

Energy equation:

$$\left(\rho C_p\right)_{nf}\left[\left(\vec{V}\cdot\nabla\right)T\right] = k_{nf}\nabla^2T + \mu_{nf}\phi + \left(\frac{D_mK_T}{C_sC_p}\right)\nabla^2T + \sigma_{nf}B_o^2E_o^2 - \sigma_{nf}B_o^2\vec{V} + 2\sigma_{nf}B_o^2E_o\,\vec{V}. \tag{3}$$

Concentration equation:

$$\left(\vec{V}\cdot\nabla\right)C = \mathrm{D_m}\nabla^2C + \frac{K_T}{T_m}\nabla^2T. \tag{4}$$

We know that the body force term corresponding to a magnetohydrodynamics (MHD) flow is the Lorentz force $\left(\vec{J}\times\vec{B}\right)$, and this Lorentz force by Hussanan *et al.* [37] becomes

$$\left(\vec{J}\times\vec{B}\right) = -\sigma_{nf}B_o^2\,\vec{V}. \tag{5}$$

Here σ_{nf} is the nanofluid electrical conductivity, B_o is the assessed magnetic field, and the velocity vector V. We know that the dynamic viscosity of nanofluid, effective density of nanofluid, thermal expansion coefficient of nanofluid, heat capacity of nanofluid, thermal diffusivity, and thermal conductivity of nanofluid are:

$$\mu_{nf} = \frac{\mu_f}{(1-\phi)^{2.5}}, \tag{6}$$

$$\rho_{nf} = (1-\phi)\rho_f + \phi\rho_s = \left(1-\phi+\phi\,\frac{\rho_s}{\rho_f}\right)\rho_f, \tag{7}$$

$$(\rho\beta)_{nf} = (1-\phi)(\rho\beta)_f + \phi(\rho\beta)_s = \left(1-\phi+\phi\,\frac{(\rho\beta)_s}{(\rho\beta)_f}\right)(\rho\beta)_f, \tag{8}$$

$$\sigma_{nf} = (1-\phi)\sigma_f + \phi\sigma_s = \left(1-\phi+\phi\,\frac{\sigma_s}{\sigma_f}\right)\sigma_f \tag{9}$$

$$\left(\rho C_p\right)_{nf} = (1-\phi)\left(\rho C_p\right)_f + \phi\left(\rho C_p\right)_s = \left(1-\phi+\phi\,\frac{\left(\rho C_p\right)_s}{\left(\rho C_p\right)_f}\right)\left(\rho C_p\right)_f, \tag{10}$$

$$\alpha_{nf} = \frac{K_{nf}}{\left(\rho C_p\right)_{nf}}, \tag{11}$$

$$k_{nf} = \left[\frac{k_s+2k_f-2\phi(k_f-k_s)}{k_s+2k_f+\phi(k_f-k_s)}\right]k_f. \tag{12}$$

Now, according to Newton's law of viscosity, according to Fourier's law of heat conduction, and also according to Fick's law of species diffusion, can be reduced as [2]

$$\frac{1}{(1-\phi)^{2.5}}\,\mu_f\left[\frac{\partial^2V}{\partial X^2}+\frac{\partial^2V}{\partial Y^2}\right] + \left[1-\phi+\phi\,\frac{(\rho\beta)_s}{(\rho\beta)_f}\right]g\rho_f\,\beta_f(T-T_o) + \left[1-\phi+\phi\,\frac{(\rho\beta)_s}{(\rho\beta)_f}\right]g\rho_f\,\beta_f(C-C_o) - \left[1-\phi+\phi\,\frac{\sigma_s}{\sigma_f}\right]\sigma_fB_o^2V + \left[1-\phi+\phi\,\frac{\sigma_s}{\sigma_f}\right]\sigma_fB_o^2E_o = 0, \tag{13}$$

$$\left[\frac{k_s+2k_f-2\phi(k_f-k_s)}{k_s+2k_f+\phi(k_f-k_s)}\right]k_f\left[\frac{\partial^2T}{\partial X^2}+\frac{\partial^2T}{\partial Y^2}\right] + \frac{1}{(1-\phi)^{2.5}}\,\mu_f\left[\left(\frac{\partial V}{\partial X}\right)^2+\left(\frac{\partial V}{\partial Y}\right)^2\right] + \frac{D_mK_T}{C_SC_P}\left[\frac{\partial^2C}{\partial X^2}+\frac{\partial^2C}{\partial Y^2}\right] + \left[1-\phi+\phi\,\frac{\sigma_s}{\sigma_f}\right]\sigma_fB_o^2E_o^2 + \left[1-\phi+\phi\,\frac{\sigma_s}{\sigma_f}\right]\sigma_fB_o^2V^2 - 2\left[1-\phi+\phi\,\frac{\sigma_s}{\sigma_f}\right]\sigma_fB_o^2E_oV = 0, \tag{14}$$

$$D_m\left[\frac{\partial^2C}{\partial X^2}+\frac{\partial^2C}{\partial Y^2}\right] + \frac{K_T}{T_m}\left[\frac{\partial^2T}{\partial X^2}+\frac{\partial^2T}{\partial Y^2}\right] = 0. \tag{15}$$

Equations (13), (14), and (15) are solved employing the following boundary conditions:

$$V = 0, T = T_1, C = C_1\ at\ Y = 0\ for\ 0 \le X \le b,$$

$$V = 0, T = T_2, C = C_2\ at\ Y = a\ for\ 0 \le X \le b,$$

$$V = 0, \frac{\partial T}{\partial X} = 0, \frac{\partial C}{\partial X} = 0 \; at \; X = 0 \; for \; 0 \le Y \le a,$$
$$V = 0, \frac{\partial T}{\partial X} = 0, \frac{\partial C}{\partial X} = 0 \; at \; X = b \; for \; 0 \le Y \le a. \tag{16}$$

The dimensionless variables are given below:

$$x = \frac{X}{a}, y = \frac{Y}{a}, v = \frac{V\rho_f a}{\mu_f}, \theta = \frac{T - T_o}{T_2 - T_1}, c = \frac{C - C_o}{C_2 - C_1}, T_o = \frac{T_1 + T_2}{2}, C_o = \frac{C_1 + C_2}{2}, A = \frac{b}{a}. \tag{17}$$

Now given in equation (17), employed in the governing equations (13), (14), and (15), and after solving, we have

$$\left[\frac{\partial^2 v}{\partial x^2} + \frac{\partial^2 v}{\partial y^2}\right] + A_1\theta + A_2 c - A_3 v + A_4 = 0, \tag{18}$$

$$\left[\frac{\partial^2 \theta}{\partial x^2} + \frac{\partial^2 \theta}{\partial y^2}\right] + A_5\left[\left(\frac{\partial v}{\partial x}\right)^2 + \left(\frac{\partial v}{\partial y}\right)^2\right] + A_6\left[\frac{\partial^2 c}{\partial x^2} + \frac{\partial^2 c}{\partial y^2}\right] + A_7(E - v)^2 = 0, \tag{19}$$

$$\left[\frac{\partial^2 c}{\partial x^2} + \frac{\partial^2 c}{\partial y^2}\right] + A_8\left(\frac{\partial^2 \theta}{\partial x^2} + \frac{\partial^2 \theta}{\partial y^2}\right) = 0. \tag{20}$$

where $G_r = \frac{g\rho_f^2\beta_f(T_2 - T_1)a^3}{\mu_f^2}$ is the thermal Grashof number, which is the ratio of thermal buoyancy force to viscous force, $G_c = \frac{g\rho_f^2\beta_f(C_2 - C_1)a^3}{\mu_f^2}$ is the solutal Grashof number, which is the ratio of species buoyancy force to the viscous hydrodynamic force, $H_a = B_o a\sqrt{\frac{\sigma_f}{\mu_f}}$ is the Hartmann number, which is the proportion of electromagnetic force to viscous force, $E = E_o\frac{\rho_f a}{\mu_f}$ is the electrical field load parameter, $B_r = \frac{\mu_f^3}{k_f\rho_f^2(T_2 - T_1)a^2}$ is the Brinkman number, and $D_f = \frac{D_m K_T(C_2 - C_1)}{\nu_f C_s C_p(T_2 - T_1)}$ is the Dufour number, which is the ratio of the concentration difference to the temperature difference. Also, $P_r = \frac{\nu_f}{k_f}$ is the Prandtl number, which is the ratio of kinematic viscosity to the thermal conductivity, $S_r = \frac{K_T(T_2 - T_1)}{\nu_f T_m(C_2 - C_1)}$ is the Soret number, which is the ratio of the temperature difference to the concentration, $S_c = \frac{\nu_f}{D_m}$ is the Schmidt number, the ratio of the momentum diffusivity (kinematic viscosity) to the mass diffusivity.

The corresponding boundary conditions after introducing equation (16) give

$$v = 0, \theta = -0.5, c = -0.5 \; at \; y = 0 \; for \; 0 \le x \le A,$$
$$v = 0, \theta = 0.5, c = 0.5 \; at \; y = 1 \; for \; 0 \le x \le A,$$
$$v = 0, \frac{\partial \theta}{\partial x} = 0, \frac{\partial c}{\partial x} = 0 \; at \; x = 0 \; and \; x = A \; for \; 0 \le y \le 1. \tag{21}$$

Let

$$E_1 = (1 - \phi)^{2.5}, E_2 = \left(1 - \phi + \phi\frac{\rho_s}{\rho_f}\right), E_3 = \left(1 - \phi + \phi\frac{(\rho\beta)_s}{(\rho\beta)_f}\right),$$
$$E_4 = (1 - \phi + \phi\frac{\sigma_s}{\sigma_f}), E_5 = \left(1 - \phi + \phi\frac{(\rho C_p)_s}{(\rho C_p)_f}\right), E_6 = \left[\frac{k_s + 2k_f - 2\phi(k_f - k_s)}{k_s + 2k_f + \phi(k_f - k_s)}\right].$$

3. NUMERICAL TECHNIQUE AND GRID INDEPENDENCE STUDY

The system of governing equations from (18) to (20), in conjunction with the boundary conditions as defined in equations (21), is solved through the application of a finite difference method. Uniform grids (Fig. 2) are generated for the computational domain. The domain of definition is portioned uniformly into M_x and M_y divisions along the x and y axes respectively. Central differencing of second-order accuracy is employed for the first and second-order derivatives. The equations (18), (19), and (20), along with the boundary conditions given in equation (21), were discretized using the finite-difference method. We know that the finite difference is second order $\partial^2 v/\partial x^2$ and first order $\partial v/\partial x$, were discretized as $\frac{\partial^2 v}{\partial x^2} = \frac{v_{i+1,j} - 2v_{i,j} + v_{i-1,j}}{\Delta x^2} + O(\Delta x^2)$ and $\frac{\partial v}{\partial x} = \frac{v_{i+1,j} - v_{i-1,j}}{2\Delta x} + O(\Delta x^2)$, respectively. Therefore, the resultant difference equations give

$$v_{i,j} = A_9\left(v_{i+1,j} + v_{i-1,j}\right) + A_{10}\left(v_{i,j_{+1}} + v_{i,j_{-1}}\right) + A_{11}\left(T_{i,j}\right) + A_{12}\left(c_{i,j}\right) + A_{13}. \tag{22}$$

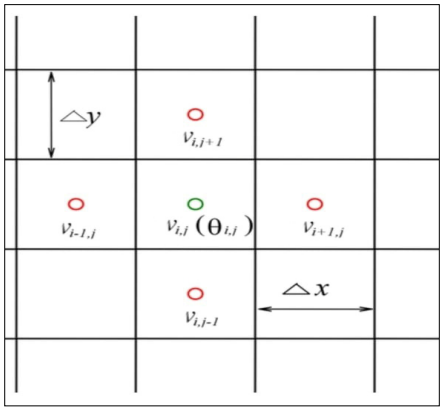

Figure 2. Uniform grid system

$$T_{i,j} = A_{14}\left(T_{i_{+1},j} + T_{i_{-1},j}\right) + A_{15}\left(T_{i,j_{+1}} + T_{i,j_{-1}}\right) + A_{16}\left(v_{i_{+1},j} - v_{i_{-1},j}\right)^2 + A_{17}\left(v_{i,j_{+1}} - v_{i,j_{-1}}\right)^2 + A_{18}\left(c_{i_{+1},j} - 2c_{i,j} + c_{i_{-1},j}\right) + A_{19}\left(c_{i,j_{+1}} - 2c_{i,j} + c_{i,j_{-1}}\right) + A_{20}\left(E - v_{i,j}\right)^2. \quad (23)$$

$$c_{i,j} = A_{14}\left(c_{i_{+1},j} + c_{i_{-1},j}\right) + A_{15}\left(c_{i,j_{+1}} + c_{i,j_{-1}}\right) + A_{21}\left(\theta_{i_{+1},j} - 2\theta_{i,j} + \theta_{i_{-1},j}\right) + A_{22}\left(\theta_{i,j_{+1}} - 2\theta_{i,j} + \theta_{i,j_{-1}}\right). \quad (24)$$

where:

$A_1 = \frac{E_3}{E_1}Gr, A_2 = \frac{E_3}{E_1}Gc, A_3 = \frac{E_4}{E_1}Ha^2, A_4 = \frac{E_4}{E_1}Ha^2E, A_5 = \frac{E_1}{E_6}Br, A_6 = \frac{1}{E_6}D_fPr, A_7 = \frac{E_4}{E_6}BrHa^2, A_8 = SrSc, A_9 = \frac{k^2}{2(k^2+h^2+A_3h^2k^2)}, A_{10} = \frac{h^2}{2(k^2+h^2+A_3h^2k^2)}$, $A_{11} = \frac{A_1h^2k^2}{(k^2+h^2+A_3h^2k^2)}$, $A_{12} = \frac{A_2h^2k^2}{(k^2+h^2+A_3h^2k^2)}$, $A_{13} = \frac{A_4h^2k^2}{(k^2+h^2+A_3h^2k^2)}, A_{14} = \frac{k^2}{2(k^2+h^2)}$, $A_{15} = \frac{h^2}{2(k^2+h^2)}$, $A_{16} = A_5 \cdot \frac{k^2}{4(k^2+h^2)}$, $A_{17} = A_5 \cdot \frac{h^2}{4(k^2+h^2)}$, $A_{18} = A_6A_{14}, A_{19} = A_6A_{15}, A_{20} = \frac{A_7h^2k^2}{(k^2+h^2)}, A_{21} = A_8A_{14}, A_{22} = A_8A_{15}$ are constants. $\Delta x = h \; and \; \Delta y = k$.

Finally, we get the discretized boundary conditions:

$$v_{i,0} = -v_{i,1}, \theta_{i,0} = -1 - \theta_{i,1}, \; c_{i,0} = -1 - c_{i,1}$$
$$v_{i,My_{+1}} = -v_{i,My}, \theta_{i,My_{+1}} = 1 - \theta_{i,My}, c_{i,My_{+1}} = 1 - c_{i,My}$$
$$v_{0,j} = -v_{1,j}, \; \theta_{0,j} = \theta_{1,j}, \; c_{0,j} = c_{1,j}$$
$$v_{Mx_{+1},j} = -v_{Mx,j}, \theta_{Mx_{+1},j} = \theta_{Mx,j}, \; c_{Mx_{+1},j} = c_{Mx,j}. \quad (25)$$

Here i goes from 1 to M_x and j 1 to M_y.

4. RESULTS AND DISCUSSION

The flow of copper (Cu), silver (Ag), titanium oxide (TiO_2), and copper oxide (CuO) nanoparticles with water (H_2O) as base fluid in a vertical rectangular duct has been studied in this work. The influence of parameters like the thermal Grashof number G_r, solutal Grashof number G_c, Hartmann number H_a, nanoparticle volume fraction ϕ, electrical field load parameter E and the Brinkmann parameter B_r in a vertical rectangular duct, the velocity, temperature, and nanoparticle concentration profiles are presented graphically. In this plotting, we have employed an explicit finite-difference scheme in MATLAB. The outcomes of this work are presented in terms of the effects of different copper nanoparticles (Cu), silver (Ag), titanium oxide (TiO_2), and copper oxide (CuO), the thermal Grashof number $(0.5 \leq G_r \leq 20)$, solutal Grashof number $(0.5 \leq G_c \leq 15)$, electric field load parameter $(-2 \leq E \leq 2)$, Brinkmann parameter $(0 \leq B_r \leq 2.5)$, solid volume fraction $(0 \leq \phi \leq 0.06)$ are shown in the velocity, temperature, and nanoparticle concentration profiles.

Verification of the result:

Since no directly analogous literature is accessible for this specific configuration, endorsement of the result is accomplished through physical reasoning and consistency with established magnetohydrodynamic (MHD) theory. The effects of Hartmann number, which is responsible for the application of a magnetic field on the velocity profile, are reported in Fig. 7. From this figure, it is perceived that the velocity distribution of the fluid has been diminished with the increasing values of Hartmann number (Ha). Physically, an increase in the Hartmann number intensifies the Lorentz force, which acts as a resistive drag on the fluid motion. Consequently, the fluid velocity decreases, which is consistent with classical MHD flow behavior.

We have taken $H_a = 2, A = 2.5, P_r = 6.93, R_m = 1, Ec = 0.001, h = k = 0.001, m = n = 200, \phi = 0.02, k_f = 0.613, k_s = 429, \theta = \pi/2$. We have plotted (Fig. 3, Fig. 4, and Fig. 5) the velocity profile, temperature profile, and concentration profile for various values of G_r and water-based floodplain copper nanoparticles. In these plots, we have

observed that the velocity of the Cu-water nanofluid increases with the increase of G_r. With these significant values of thermal Grashof number G_r, buoyancy force control, and on the other hand, due to small values of thermal Grashof number G_r, viscosity control, i.e., profile velocity stimulated by the buoyancy force. Due to thermal buoyancy, an increase in G_r tends to produce stronger flow in the boundary layer. However, in the temperature and concentration profiles, we have noticed that they are invariant, which is mainly due to the neglect of viscous dissipation in the energy equation. We have plotted the velocity profile (Fig. 6) for different values of G_c and a water-based nanofluid employing copper nanoparticles.

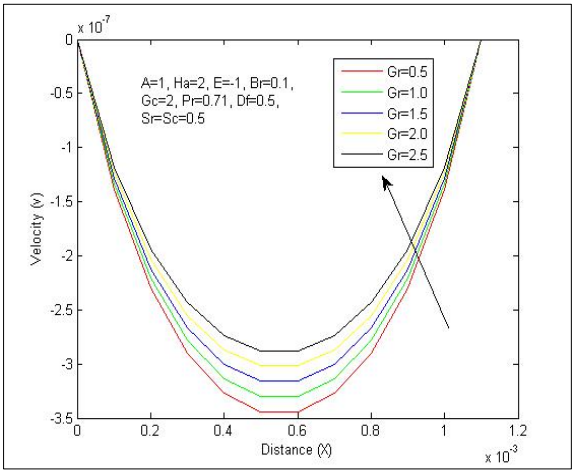

Figure 3. Variation in (v) with G_r

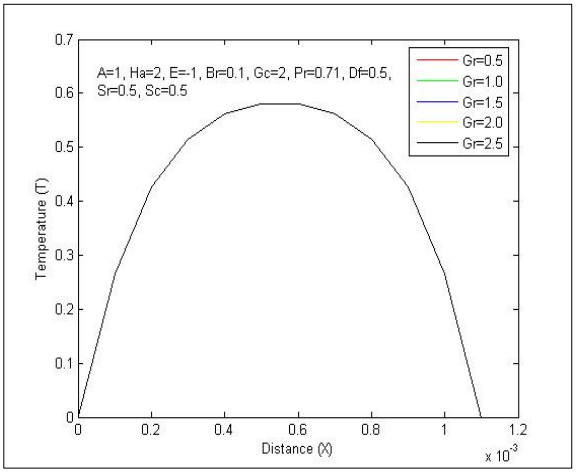

Figure 4. Variation in (T) with G_r

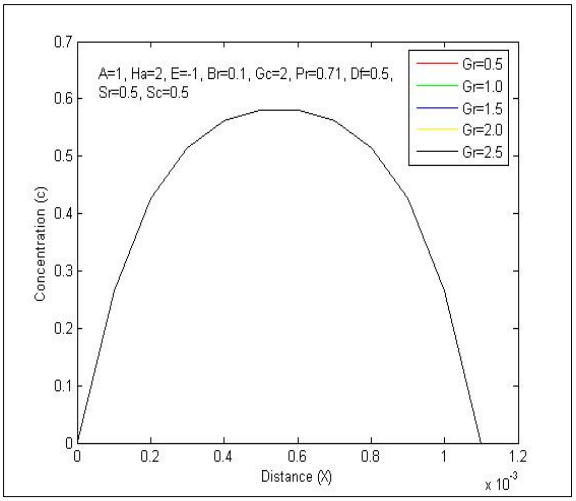

Figure 5. Variation in (c) with G_r

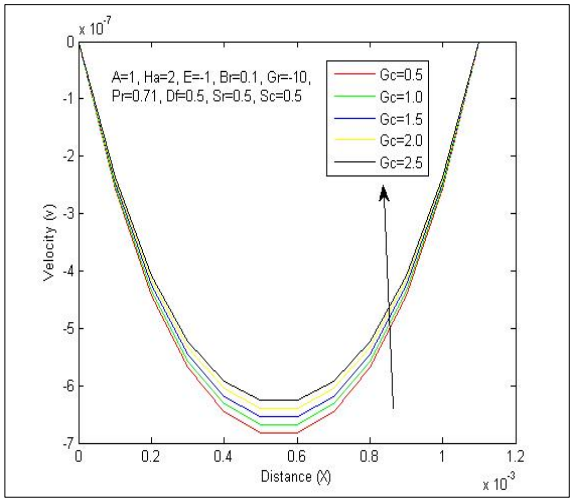

Figure 6. Variation in (v) with G_c

In these plots, we have observed that the profile velocity with copper-water nanofluid enhances due to the increase in G_c, with the most significant values of solutal Grashof number cap G_c, species hydrodynamic buoyancy force control, and on the other hand, due to small values of solutal Grashof number G_c, viscosity control. Due to the effect of thermal buoyancy, an increase in the values of G_c tends to produce a large amount of flow in the boundary layer. The temperature and concentration profiles are not displayed graphically because they exhibit topologies similar to those of the thermal Grashof number G_r. We have plotted (Fig. 7) the velocity profile in the boundary layer for distinct values of the Hartmann number H_a, and for a water-based nanofluid employing copper nanoparticles. In these plots (Fig. 7), we observe that the flow rate decreases with increasing Hartmann number H_a when copper nanoparticles are present, due to the enhanced H_a. The magnetic field introduced into the electrically conducting nanofluid, acting normal to the boundary, generates a resistive pressure force in the duct, which is part of the Lorentz force. The temperature and concentration profiles are not displayed graphically because they exhibit topologies similar to those of the thermal Grashof number G_r. We have plotted (Fig. 8) the velocity in the boundary layer for different values of nanoparticle volume fraction ϕ, using water as the base fluid and employing copper nanoparticles. In these plots, we observe that the flow rate of the nanoparticle volume fraction phi with copper nanoparticles increases as ϕ increases. The temperature and concentration profiles are not displayed graphically, as they exhibit topologies similar to those of the temperature and concentration profiles for the thermal Grashof number G_r.

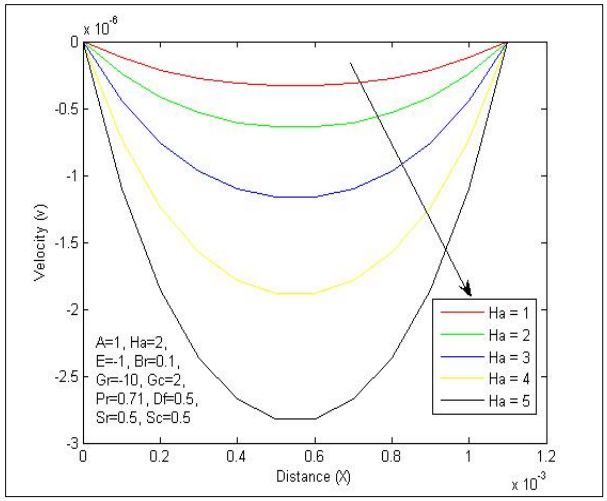

Figure 7. Variation in (v) with H_a

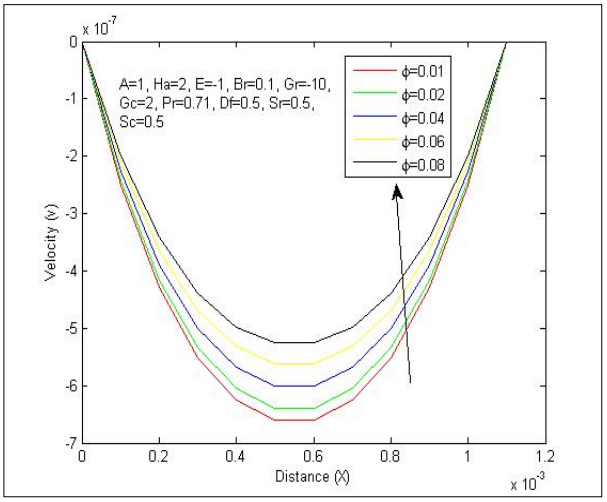

Figure 8. Variation in (v) with ϕ

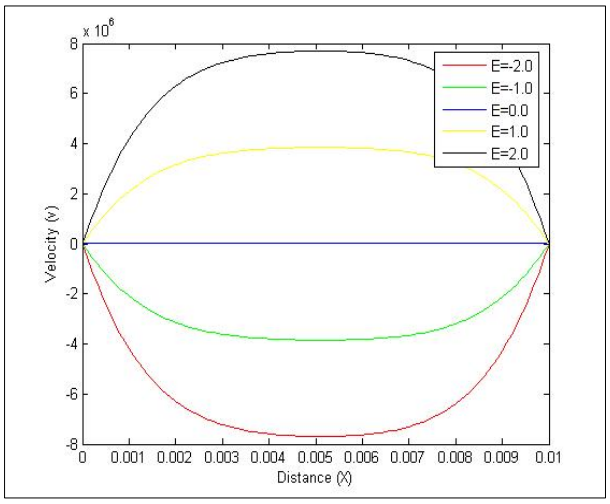

Figure 9. Variation in (v) with E

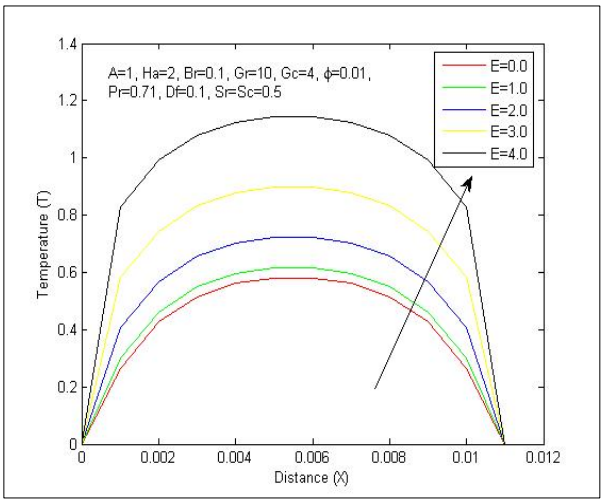

Figure 10. Variation in (T) with E

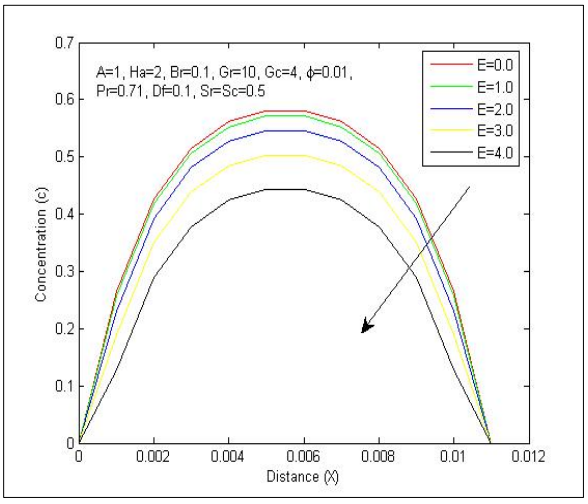

Figure 11. Variation in (c) with E

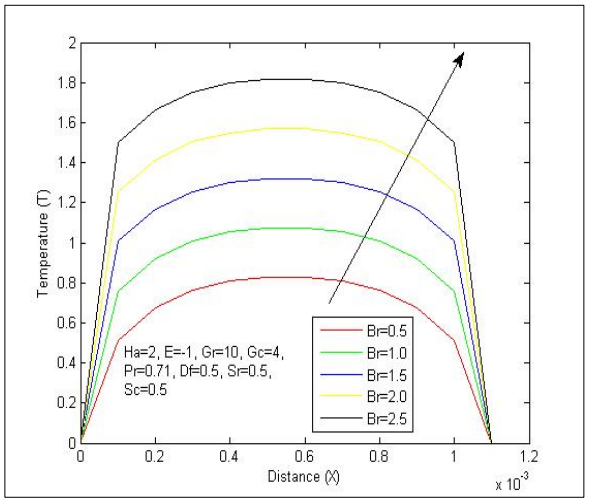

Figure 12. Variation in (T) with B_r

We have plotted (Fig. 9, Fig. 10, and Fig. 11) for velocity, temperature, and concentration profiles in the boundary layer for different values of electrical field load parameter E, base fluid water employing copper nanoparticles. In these plottings, we have noticed that the velocity of Cu −water nanofluid enhances due to the enhancement of electrical field

load parameter E. i.e, flow is accelerated due to the enhancement in electrical field load parameter E. Similarly, in the temperature profile of Cu −water nanofluid we have observed that this profile is also enhance due to the enhancement of electrical field load parameter E. However, in the concentration profile of the Cu −water nanofluid, we observed a decrease in concentration with increasing electrical field load parameter E. We have plotted (Fig. 12) the temperature and concentration profiles in the boundary layer for different values of the Brinkmann number B_r, for a base fluid of water containing copper nanoparticles. On the contrary, in the temperature profile, we have observed that it increases with increasing Brinkman number B_r. However, it was observed that, with an increase in the Brinkman number B_r, the boundary-layer thickness decreased at all points. The velocity profile is not displayed graphically because it exhibits a topology similar to that of the thermal Grashof number G_r.

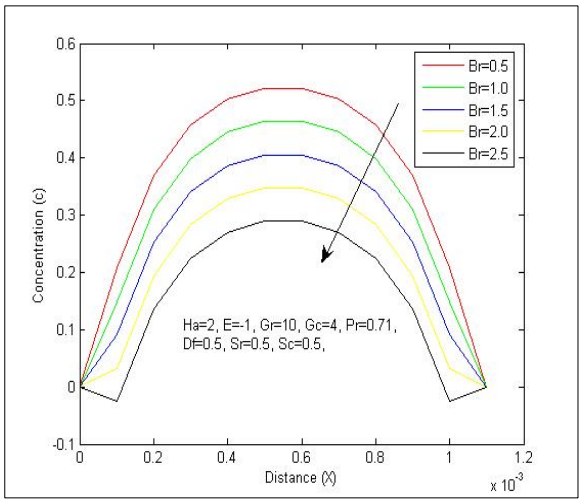

Figure 13. Variation in (c) with B_r

Case I for copper/water nanofluid:

Sl. No.	G_c	Leading value of velocity	Rate of increase of the leading value of velocity for different Solutal Grashof number G_c
	G_i	L_i	$R_i = \frac{L_{i+1} - L_i}{L_i}$
1	$G_1 = 0.10$	$L_1 = -6.10$	$R_1 = -0.0163934426$
2	$G_2 = 0.20$	$L_2 = -6.20$	$R_2 = -0.0161290323$
3	$G_3 = 0.30$	$L_3 = -6.30$	$R_3 = -0.0158730159$
4	$G_4 = 0.40$	$L_4 = -6.40$	$R_4 = -0.0156250000$
5	$G_5 = 0.50$	$L_5 = -6.50$	$R_5 = -0.0153846154$
6	$G_6 = 0.60$	$L_6 = -6.60$	$R_6 = -0.0151515152$
7	$G_7 = 0.70$	$L_7 = -6.70$	$R_7 = -0.0149253731$
8	$G_8 = 0.80$	$L_8 = -6.80$	$R_8 = -0.0147058824$
9	$G_9 = 0.90$	$L_9 = -6.90$	$R_9 = -0.0144927536$
10	$G_{10} = 1.00$	$L_{10} = -7.00$	

Case II: For silver/water nanofluid:

Sl. No.	G_c	Leading value of velocity	Rate of increase of the leading value of velocity for different Solutal G_c
	G_i	L_i	$R_i = \frac{L_{i+1} - L_i}{L_i}$
1	$G_1 = 0.10$	$L_1 = -8.10$	$R_1 = -0.0123456790$
2	$G_2 = 0.20$	$L_2 = -8.20$	$R_2 = -0.0121951220$
3	$G_3 = 0.30$	$L_3 = -8.30$	$R_3 = -0.0120481928$
4	$G_4 = 0.40$	$L_4 = -8.40$	$R_4 = -0.0119047619$
5	$G_5 = 0.50$	$L_5 = -8.50$	$R_5 = -0.0117647059$
6	$G_6 = 0.60$	$L_6 = -8.60$	$R_6 = -0.0116279070$
7	$G_7 = 0.70$	$L_7 = -8.70$	$R_7 = -0.0114942529$
8	$G_8 = 0.80$	$L_8 = -8.80$	$R_8 = -0.0113636364$
9	$G_9 = 0.90$	$L_9 = -8.90$	$R_9 = -0.0112359551$
10	$G_{10} = 1.00$	$L_{10} = -9.00$	

Case III For titanium oxide/water nanofluid:

Sl. No.	G_c	Leading value of velocity	Rate of increase of the leading value of velocity for different Solutal G_c
	G_i	L_i	$R_i = \frac{L_{i+1} - L_i}{L_i}$
1	$G_1 = 0.10$	$L_1 = -2.70$	$R_1 = -0.0370370370$
2	$G_2 = 0.20$	$L_2 = -2.80$	$R_2 = -0.0357142857$
3	$G_3 = 0.30$	$L_3 = -2.90$	$R_3 = -0.0344827586$
4	$G_4 = 0.40$	$L_4 = -3.00$	$R_4 = -0.0333333333$
5	$G_5 = 0.50$	$L_5 = -3.10$	$R_5 = -0.0322580645$
6	$G_6 = 0.60$	$L_6 = -3.20$	$R_6 = -0.0312500000$
7	$G_7 = 0.70$	$L_7 = -3.30$	$R_7 = -0.0303030303$
8	$G_8 = 0.80$	$L_8 = -3.40$	$R_8 = -0.0294117647$
9	$G_9 = 0.90$	$L_9 = -3.50$	$R_9 = -0.0285714286$
10	$G_{10} = 1.00$	$L_{10} = -3.60$	

Case IV For copper oxide/water nanofluid:

Sl. No.	G_c	Leading value of velocity	Rate of increase of the leading value of velocity for different Solutal G_c
	G_i	L_i	$R_i = \frac{L_{i+1} - L_i}{L_i}$
1	$G_1 = 0.10$	$L_1 = -2.80$	$R_1 = -0.0357142857$
2	$G_2 = 0.20$	$L_2 = -2.90$	$R_2 = -0.0344827586$
3	$G_3 = 0.30$	$L_3 = -3.00$	$R_3 = -0.0333333333$
4	$G_4 = 0.40$	$L_4 = -3.10$	$R_4 = -0.0322580645$
5	$G_5 = 0.50$	$L_5 = -3.20$	$R_5 = -0.0312500000$
6	$G_6 = 0.60$	$L_6 = -3.30$	$R_6 = -0.0303030303$
7	$G_7 = 0.70$	$L_7 = -3.40$	$R_7 = -0.0294117647$
8	$G_8 = 0.80$	$L_8 = -3.50$	$R_8 = -0.0285714286$
9	$G_9 = 0.90$	$L_9 = -3.60$	$R_9 = -0.0277777778$
10	$G_{10} = 1.00$	$L_{10} = -3.70$	

We have plotted (Fig. 14) the rate-of-rise leading velocity for different nanofluids against the corresponding solutal Grashof number G_c, in the duct under the same configuration. We have plotted the graphs for the following nanofluids: copper (Cu) and silver (Ag), titanium oxide (TiO_2) and copper oxide (CuO). These plots provide a comparative advantage in mass transfer for different nanofluids at a given temperature. From the plots (Fig. 14), we see that as the solute Grashof number G_c increases, the difference in flow rate between the nanofluids decreases. For a low value of the solutal Grashof number G_c, gives the high flow rate, and titanium oxide (TiO_2) gives a low flow rate. For high solutal G_c, all the nanofluids considered show no significant difference in volumetric flow rate.

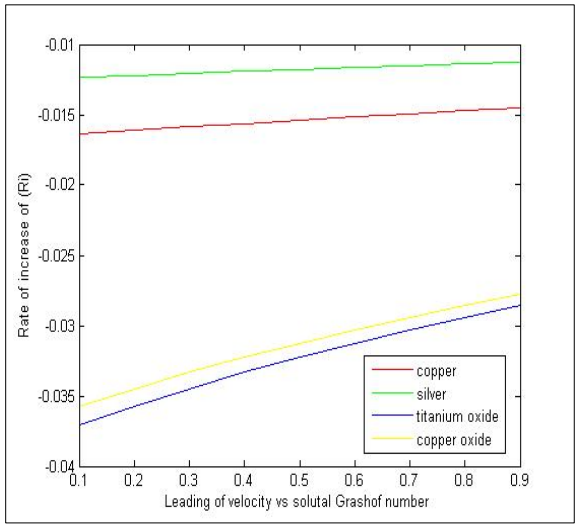

Figure 14. Rate of increase of solutal Grashof number G_c for different nanoparticles, copper (Cu), silver (Ag), titanium oxide (TiO_2) and copper oxide (CuO)

The 3D temperature distribution shows that the disk occupies the convex region, and the copper contours are more nonlinear than those of aluminum and titanium oxide. The concentration distribution and the topology are in a concave position, and the contours are much less disturbed for all the nanoparticles. For the flow concerning copper nanofluids, we have plotted the graphs in (x, y, v) mesh, (x, y, T) mesh and (x, y, c) mesh in Fig. 10. Similarly, graphs are plotted for other nanofluids of silver, aluminum, and titanium oxide in Fig. 12, Fig. 14, and Fig. 17. Further, in Fig. 11, Fig. 13, Fig. 15, and Fig. 17, we have employed 100×100 grid size for the velocity profile at $x = 1$ when $y = 0$ and we have employed 20×20 grid size for temperature and concentration profiles at $x = 1$ when $y = 1$. We have plotted velocity, temperature, and concentration profiles in the duct for Cu-water, Ag-water, and TiO_2-water nanofluids. We can get a regular profile of velocity, temperature, and concentration about the center section of the duct $(at\ x = \frac{1}{2})$.

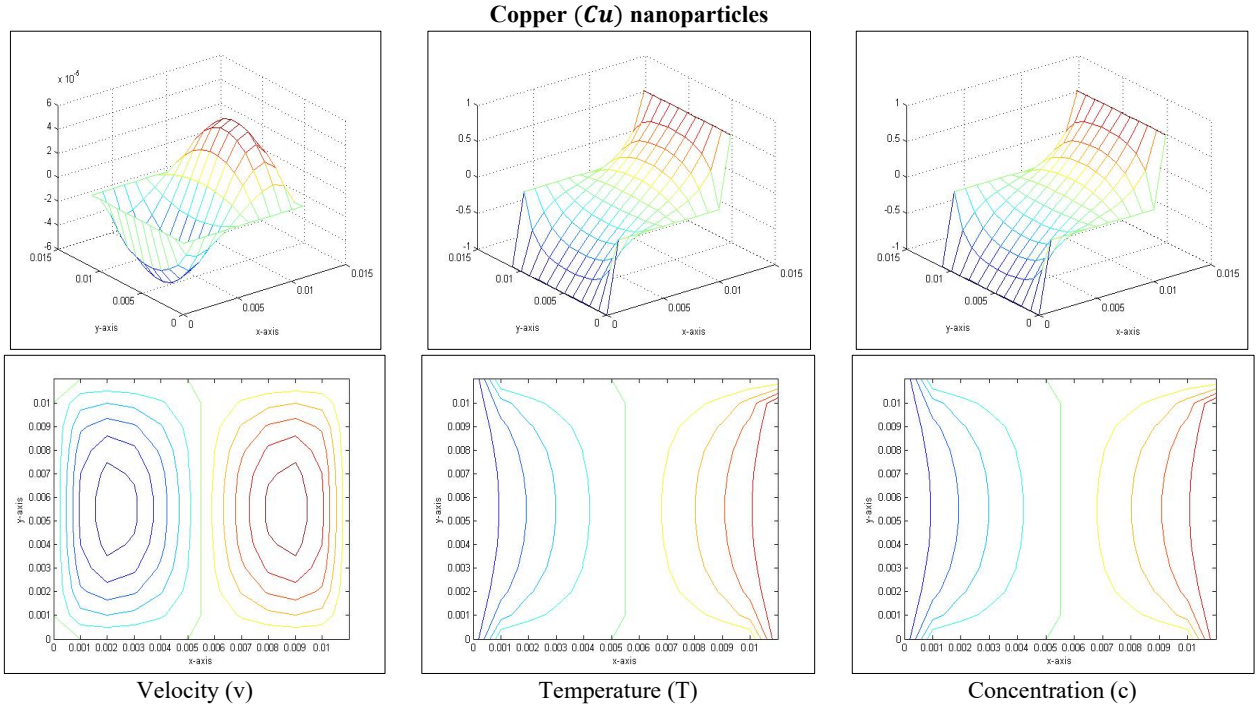

Figure 15. Velocity profile in mesh (x, y, v); Temperature profile in mesh (x, y, T) and Concentration profile in mesh (x, y, c) for copper nanoparticles

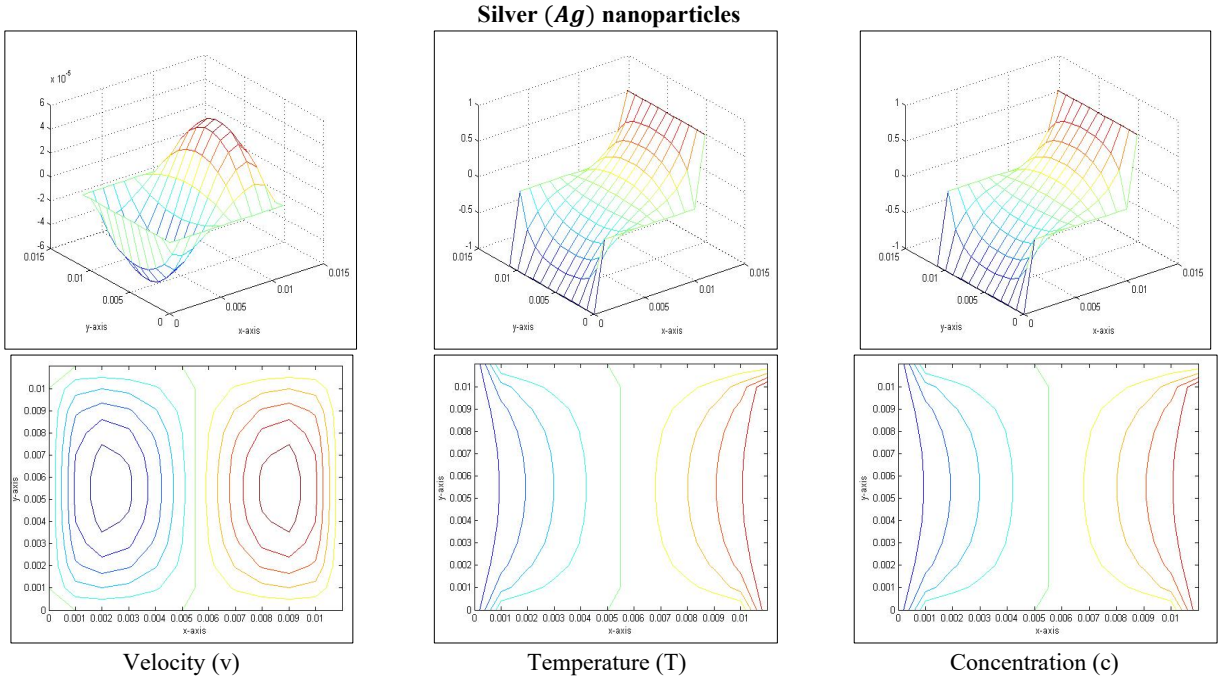

Figure 16. Velocity profile in mesh (x, y, v); Temperature profile in mesh (x, y, T) and Concentration profile in mesh (x, y, c) for silver nanoparticles

Titanium oxide (TiO_2) nanoparticles

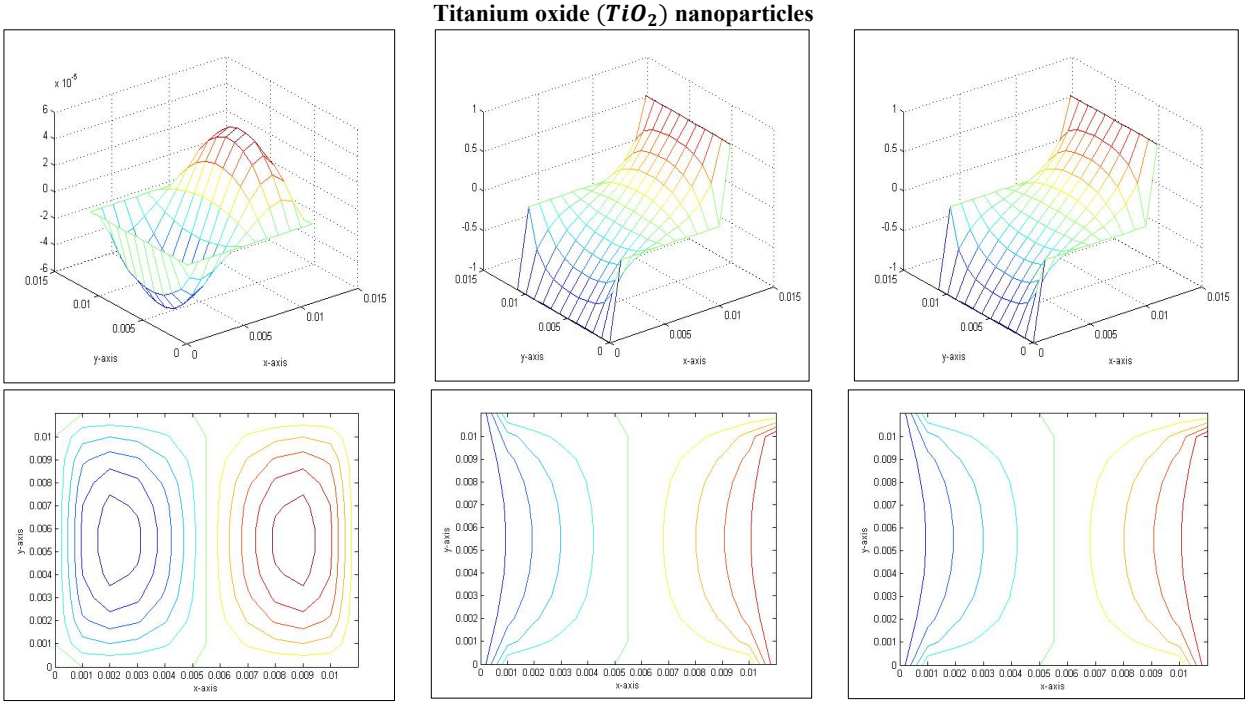

Velocity (v) Temperature (T) Concentration (c)

Figure 17. Velocity profile in mesh (x, y, v); Temperature profile in mesh (x, y, T) and Concentration profile in mesh (x, y, c) for titanium oxide nanoparticles

Copper oxide (CuO) nanoparticles

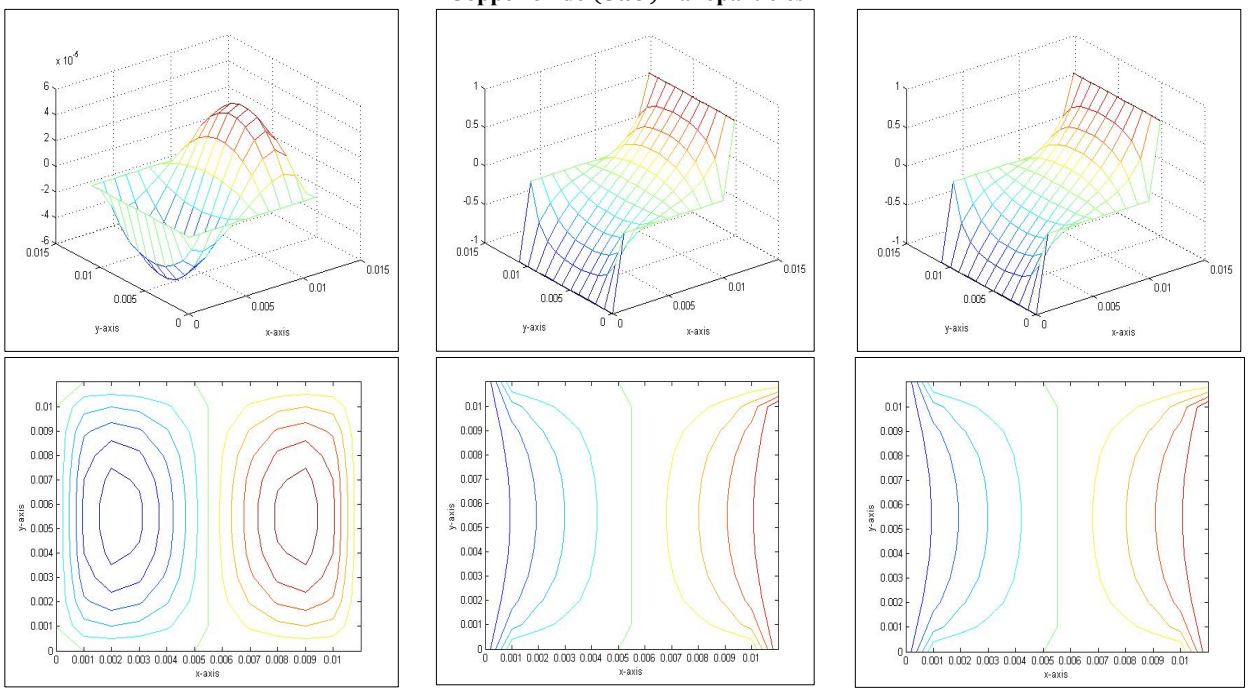

Velocity (v) Temperature (T) Concentration (c)

Figure 18. Velocity profile in mesh (x, y, v); Temperature profile in mesh (x, y, T) and Concentration profile in mesh (x, y, c) for copper oxide nanoparticles

5. CONCLUSIONS

In this work, we have studied a vertical rectangular duct in the presence of a strong transverse magnetic field, with velocity, temperature, and concentration profiles of different copper-based nanofluids (Cu) , silver (Ag), titanium oxide (TiO_2), and copper oxide (CuO) nanoparticles with water as a base fluid. The governing equations are solved using the explicit finite difference method (EFDM), also known as the second-order upwind method. The results are shown graphically for different parameter values. The computational process is carried out using MATLAB code. The following conclusions we have found from the present investigations:

1. From the plotting of (Fig. 5), we have seen that with increasing solutal Grashof number G_c. The difference in flow rate for different nanofluids is decreasing. For a low value of the solutal Grashof number G_c, titanium oxide (TiO_2) gives a high flow rate and silver (A_g) gives a low flow rate. For high solutal Grashof number G_c, all the nanofluids considered show no significant difference in volumetric flow rate.
2. For increasing values of thermal Grashof number G_r, solutal Grashof number G_c, electrical field load parameter E and the nanoparticle volume fraction ϕ. The fluid velocity also increases. But with the increasing values of the Hartmann number H_a, the velocity decreases in copper-water nanofluids.
3. With the increasing values of the electrical field load parameter E and the Brinkmann number B_r, the temperature and concentration profiles are found to increase due to an increase in the values of the electrical field load parameter E and Brinkmann number B_r, but the boundary layer reduces the concentration; its thickness decreases.

ORCID

Hirak Jyoti Dehingia, https://orcid.org/0000-0002-3119-0842; **Kaushik Dehingia,** https://orcid.org/0000-0002-8042-4166
Rupjyoti Borah, https://orcid.org/0000-0001-7765-7877; **Utpal Saikia,** https://orcid.org/0000-0003-0235-6871

REFERENCES

[1] S.U.S. Choi, "Enhancing thermal conductivity of fluids with nanoparticles, in developments and applications of non-Newtonian flows," ASME FED 231/MD, **66**, 99-103 (1995). https://doi.org/10.1115/imece1995-0926
[2] L. Godson, B. Raja, D.M. Lal, and S. Wongwises, "Enhancement of heat transfer using nanofluids-An overview," Renewable and Sustainable Energy Reviews, **14**, 629-641 (2010). https://doi.org/10.1016/j.rser.2009.10.004
[3] J.C. Maxwell, *A Treatise on Electricity and Magnetism*, (Clarendon Press, Oxford, UK, 1881).
[4] S. Lee, S.U.S.S. Choi, S. Li, and J.A. Eastman, "Measuring thermal conductivity of fluids containing oxide nanoparticles," ASME. J. Heat Transfer, **121**, 280-289 (1999). https://doi.org/10.1115/1.2825978
[5] J.A. Eastman, S.U.S. Choi. and S. Li, and W.L. Thompson, "Anomalously increased effective thermal conductivities of ethylene glycol-based nanofluids containing copper nanoparticles," Appl. Phys. Lett. **78**, 718-720 (2001). https://doi.org/10.1063/1.1341218
[6] Y. Xuan, and Q. Li, "Heat transfer enhancement of nanofluids," Int. J. Heat Fluid Flow, **21**, 58-64 (2000). https://doi.org/10.1016/s0142-727x(99)00067-3
[7] S.K. Das, S.U.S. Choi, W. Yu, and T. Pradet, *Nanofluids: Science and Technology*, (Wiley, New Jersey, 2007).
[8] W. Daungthongsuk, and S. Wongwises, "A critical review of convective heat transfer nanofluids," Renewable Sustainable Energy Rev. **11**, 797-817 (2007). https://doi.org/10.1016/j.rser.2005.06.005
[9] X.Q. Wang, and A.S. Mujumdar, "A review on nanofluids-part I: Theoretical and numerical investigations," Braz. J. Chem. Eng. **25**, 613-630 (2008). https://doi.org/10.1590/s0104-66322008000400001
[10] X.Q. Wang, and A.S. Mujumdar, "A review on nanofluids-part II: Experimental and application investigations," Braz. J. Chem. Eng. **25**, 631-648 (2008). https://doi.org/10.1590/s0104-66322008000400002
[11] S. Kakaç, and A. Parmuanjaroenkij, "Review of Convective Heat Transfer Enhancement with Nanofluids," International Journal of Heat Mass Transfer, **52**, 3187-3196 (2009). https://doi.org/10.1016/j.ijheatmasstransfer.2009.02.006
[12] Y. Ding. H. Chen, I. Wang, C.Y. Yang. Y. Hel W. Yang W.P. Lee, *et al*., "Heat transfer intensification using nanofluids," Kona, **25**, 3187-3196 (2007). https://doi.org/10.14356/kona.2007006
[13] I. Tavman, A. Turgut, M. Chirtoc, K. Hadjov, O. Fudym, and S. Tavman, "Experimental Study on Thermal Conductivity and Viscosity of Water-Based Nanofluids," Heat Transfer Res. **41**(3), 339-351 (2010). https://doi.org/10.1615/heattransres.v41.i3.100
[14] A. Einstein, "Correction of My Work: A New Determination of the Molecular Dimensions", Ann. Phys. **34**(3), 591-592 (1911).
[15] P.K. Namburu, D.K. Das, K.M. Tanguturi, and R.S. Vajjha, "Numerical Study of Turbulent Flow and Heat Transfer Characteristics of Nanofluids Considering Variable Properties," Int. J. Therm. Sci., **48**(2), 290-302 (2009). https://doi.org/10.1016/j.ijthermalsci.2008.01.001
[16] T. Bergman, "Effect of Reduced Specific Heats of Nanofluids on Single Phase, Laminar Internal Forced Convection," Int. J. Heat Mass Transfer, **52**(5-6), 1240-1244 (2009). https://doi.org/10.1016/j.ijheatmasstransfer.2008.08.019
[17] R. Younsi, "Computational analysis of MHD flow, heat and mass transfer in trapezoidal porous cavity," Thermal Science, **13**, 13-22 (2009). https://doi.org/10.2298/tsci0901013y
[18] P.R. Sharma, and G. Singh, "Effects of Ohmic heating and viscous dissipation on steady MHD flow near a stagnation point on an isothermal stretching sheet," Thermal Science, **13**, 5-12 (2009). https://doi.org/10.2298/tsci0901005s
[19] P.A. Vadher, G.M. Deheri, and R.M. Patel, "Performance of hydromagnetic squeeze films between conducting porous rough conical plates," Meccanica, **45**, 767-783 (2010). https://doi.org/10.1007/s11012-010-9279-y
[20] J.C. Umavathi, I.C. Liu, and M.A. Sheremet, "Convective heat transfer in a vertical rectangular duct filled with a nanofluid," Heat Transfer Asian Research, **45**, 661-679 (2016). https://doi.org/10.1002/htj.21182
[21] R. Ellahi, M. Hassan, and A. Zeeshan, "Aggregation Effects on Water-Based Al_2O_3- Nanofluid over Permeable Wedge in Mixed Convection," Asia-Pacific Journal of Chemical Engineering, **11**, 179-186 (2015). https://doi.org/10.1002/apj.1954
[22] M.A.A. Hamad, "Analytical Solution of Natural Convection Flow of a Nanofluid over a Linearly Stretching Sheet in the Presence of Magnetic Field," International Communications in Heat and Mass Transfer, **38**, 487-492 (2011). https://doi.org/10.1016/j.icheatmasstransfer.2010.12.042
[23] T. Hayat, M.B. Ashraf, S.A. Shehzad, and A. Alsaedi, "Mixed Convection Flow of Casson Nanofluid over a Stretching Sheet with Convectively Heated Chemical Reaction and Heat Source/Sink," J. Appl Fluid Mechanics, **8**, 803-813 (2015). https://doi.org/10.18869/acadpub.jafm.67.223.22995

[24] P.K. Kameswaran, M. Narayana, P. Sibanda, and P.V.S.N. Murthy, "Hydromagnetic Nanofluid Flow Due to a Stretching or Shrinking Sheet with Viscous Dissipation and Chemical Reaction Effect," International Journal of Heat and Mass Transfer, **55**, 7587-7595 (2012). https://doi.org/10.1016/j.ijheatmasstransfer.2012.07.065
[25] O.D. Makinde, and A. Aziz, "Boundary Layer Flow of a Nanofluid Past a Stretching Sheet with a Convective Boundary Condition," Int. J. Therm. Sci. **50**, 1326-1332 (2011). https://doi.org/10.1016/j.ijthermalsci.2011.02.019
[26] J.C. Umavathi, and O.A. Beg, "Computation of thermo-solutal convection with Soret-Dufour cross diffusion in a vertical duct containing carbon/metallic nanofluids," Journal of Mechanical Engineering Science, **236**(13), (2022). https://doi.org/10.1177/09544062211072693
[27] S. Nadeem, R.U. Haq, and N.S. Akbar, "MHD Three-Dimensional Boundary Layer Flow of Casson Nanofluid Past a Linearly Stretching Sheet with Convective Boundary Condition," IEEE Transactions on Nanotechnology, **13**, 109-115 (2014). https://doi.org/10.1109/tnano.2013.2293735
[28] H.F. Oztop and E. Abu-Nada "Numerical Study of Natural Convection in Partially Heated Rectangular Enclosures Filled with Nanofluids," Int. J. Heat. Mass Transf. **29**, 1326-1336 (2008). https://doi.org/10.1016/j.ijheatfluidflow.2008.04.009
[29] M.M. Rashidi, N. Vishnu Ganesh, A.K. Abdul Hakeem, and B. Ganga, "Buoyancy Effect on MHD Flow of Nanofluid Over a Stretching Sheet in the Presence of Thermal Radiation," Journal of Molecular Liquids, **198**, 234-238 (2014). https://doi.org/10.1016/j.molliq.2014.06.037
[30] M. Sheikholeslami, M.G. Bandpy, R. Ellahi, and A. Zeeshan, "Simulation of MHD CuO-Water Nanofluid Flow and Convective Heat Transfer Considering Lorentz Forces," Journal of Magnetism and Magnetic Materials, **369**, 69-80 (2014). https://doi.org/10.1016/j.jmmm.2014.06.017
[31] M. Turkyilmanzoglu, "Natural Convective Flow of Fluids Past a Radiative and Impulsive Vertical Plate," J. Aerosp. Eng. **29**, 1-8 (2016). https://doi.org/10.1061/(asce)as.1943-5525.0000643
[32] S. Rao, and P.A. Deka, "Numerical investigation on transport phenomena in a nanofluid under the transverse magnetic field over a stretching plate associated with solar radiation," in: *Nonlinear Dynamics and Applications. Springer Proceedings in Complexity*, edited by S. Banerjee and A. Saha (Springer, Cham. 2022), pp. 473-492. https://doi.org/10.1007/978-3-030-99792-2_39
[33] B.R. Das, P.N. Deka, and S. Rao, "Numerical analysis on MHD mixed convection flow of aluminum-oxide/water nanofluids in a vertical square duct," East European Journal of Physics, (2), 51-62 (2023). https://doi.org/10.26565/2312-4334-2023-2-02
[34] A. Majeed, A. Zeesham, M. Jawad, and M.S. Alhodaly, "Influence of melting heat transfer and chemical reaction on the flow of non-Newtonian nanofluid with Brownian motion: Advancement in mechanical engineering," in: *Proceedings of the Institution of Mechanical Engineers, Part E: Journal of Process Mechanical Engineering*, **238**(1), (2022). https://doi.org/10.1177/09544089221145527
[35] M. Jawad, M.K. Hameed, K.S. Nisar, and A.H. Majeed, "Darcy-Forchheimer flow of Maxwell nanofluid flow over a porous stretching sheet with Arrhenius activation energy and Nield boundary conditions," Case Studies in Thermal Engineering, **44**, 102830 (2023). https://doi.org/10.1016/j.csite.2023.102830
[36] M. Jawad, and K.S. Nisar, "Upper-convected flow of Maxwell fluid near stagnation points through porous surface using Cattaneo-Chrisov heat flux model," Case Studies in Thermal Engineering," **48**, 103155 (2023). https://doi.org/10.1016/j.csite.2023.103155
[37] A. Hussanan, Z. Ismail, I. Khan, A.G. Hussein, and S. Shafie, "Unsteady boundary layer MHD free convection flow in a porous medium with constant mass diffusion and Newtonian heating," Eur. Phys. J. Plus, **129**(3), 46 (2014). https://doi.org/10.1140/epjp/i2014-14046-x

МГД КАНАЛЬНИЙ ПОТОК НАНОРІДИНИ ПІД ВПЛИВОМ ПОДВІЙНОГО ДЖЕРЕЛА ТЕПЛА ЗА НАЯВНОСТІ ЕЛЕКТРИЧНОГО (E_o) ТА МАГНІТНОГО (B_o) ПОЛІВ

Бішну Рам Дас[1], Хірак Джйоті Дехінгія[2], Каушік Дехінгія[3,4], Рупджйоті Бора[5], Утпал Саікія[6]

[1]Департамент математики, коледж BCM, Камруп-781102, Ассам, Індія
[2]Відділ фундаментальних і гуманітарних наук, DUIET, Університет Дібругарх, Дібругарх, Ассам, Індія, 786004
[3]Департамент математики, коледж Сонарі, Чарайдео, Ассам, Індія, 785690
[4]Дослідницький центр прикладної математики, Хазарський університет, Баку, Азербайджан, AZ1096
[5]Департамент математики, коледж Тінгхонг, Тінгхонг-786612, Дібругарх, Ассам, Індія
[6]Департамент математики, Політехнічний університет Ґолагхат, 785610, Фуркатінг, Голагхат, Ассам, Індія

У цьому дослідженні розглядається потік наночастинок міді (Cu), срібла (Ag), оксиду титану (TiO_2), оксиду міді (CuO) з водою як основною рідиною в присутності сильного магнітного поля у вертикальному прямокутному каналі. Ліва та права стінки каналу підтримуються при різних стаціонарних температурах та концентраціях. Поля температури, швидкості та концентрації наночастинок описуються рівняннями переносу. Для дискретизації зв'язаних нелінійних рівнянь Нав'є-Стокса використовується метод проти вітру другого порядку, явний метод скінченних різниць (EFDM). Щоб дослідити ефективність теплопередачі цієї нанорідини, ми знерозмірили визначальні рівняння та отримали рішення за допомогою явної числової схеми. Для виконання обчислювальних кроків використовується код MATLAB. Ми побудували графіки полів швидкості, температури та концентрації для різних значень магнітогідродинамічних (МГД) параметрів потоку, включаючи теплове число Грасгофа (G_r), розчинне число Грасгофа (G_c), число Гартмана (H_a), параметр навантаження електричного поля (E), число Брінкмана (B_r) та об'ємну частку наночастинок (ϕ).

Ключові слова: *електричне поле; магнітне поле; нанорідини; нелінійність; явний метод скінченних різниць (EFDT); прямокутний вертикальний канал; МГД-потік; сила плавучості; в'язкий потік*